Meccanica (2013) 48:33–43
DOI 10.1007/s11012-012-9581-y

Effect of local thermal non-equilibrium on unsteady heat transfer by natural convection of a nanofluid over a vertical wavy surface

Sameh E. Ahmed · M.M. Abd El-Aziz

Received: 22 October 2011 / Accepted: 31 July 2012 / Published online: 16 August 2012

Abstract This paper uses thermal non-equilibrium model to study transient heat transfer by natural convection of a nanofluid over a vertical wavy surface. The model used for the nanofluid incorporates the effects of Brownian motion and thermophoresis. Three-temperature model is applied to represent the local thermal non-equilibrium among the particle, fluid, and solid-matrix phases. Finite difference method is used to solve the dimensionless governing equations of the problem. The obtained results are displayed in 2D graphs to illustrate the influences of the different physical parameters on local skin-friction coefficient, local Nusselt numbers for fluid, particle and solid phases and local Sherwood number. The results for velocity component, nanoparticle volume fraction, fluid temperature, particle temperature and solid-matrix temperature are presented in 3D graphs as a function of the axial and transverse coordinates. All the obtained results are discussed.

Keywords Nanofluid · Wavy surface · Transient analysis · Non-equilibrium model

Nomenclature

$\bar{a}$	dimensional amplitude of the wavy surface
A	amplitude-wave length ratio, $\bar{a}/L$
C_f	local skin-friction coefficient, defined by Eq. (43)
Da	Darcy number, defined by Eq. (16)
D_B	Brownian diffusion coefficient
D_T	thermophoretic diffusion coefficient
g	gravitational acceleration
h_{fp}	heat transfer coefficient for fluid/particle interface
h_{fs}	heat transfer coefficient for fluid/solid interface
k	thermal conductivity
K	permeability of the porous medium
L	wavelength of the wavy surface
Le	Lewis number, defined by Eq. (18)
N_b	Brownian motion parameter, defined by Eq. (20)
N_r	buoyancy ratio, defined by Eq. (19)
N_t	thermophoresis parameter, defined by Eq. (21)
N_{hp}	Nield number for the fluid/particle interface, defined by Eq. (22)
N_{hs}	Nield number for the fluid/solid interface, defined by Eq. (23)
Nu_x	local Nusselt number, defined by Eqs. (37)–(39)
P	pressure
Pr	Prandtl number, defined by Eq. (17)
Ra	Rayleigh number, defined by Eq. (15)
Sh	Sherwood number, defined by Eq. (40)
t	dimensional time
T	dimensional temperature

S.E. Ahmed (✉) · M.M. Abd El-Aziz
Department of Mathematics, Faculty of Sciences, South Valley University, Qena, Egypt
e-mail: sameh_sci_math@yahoo.com

V velocity vector
u, v dimensional velocity components
$\bar{u}, \bar{v}$ dimensionless velocity components, defined by Eq. (7)
$\tilde{U}$ characteristic velocity
x, y dimensional Cartesian coordinates
$\bar{x}, \bar{y}$ dimensionless Cartesian coordinates, defined by Eq. (7)

Greek symbols

α thermal diffusivity
β volumetric expansion coefficient for the fluid
γ_p modified thermal capacity ratio, defined by Eq. (24)
γ_s modified thermal capacity ratio, defined by Eq. (25)
ε porosity
ε_p modified thermal diffusivity ratio, defined by Eq. (26)
ε_s modified thermal diffusivity ratio, defined by Eq. (27)
μ viscosity of the fluid
ρ density
(ρc) heat capacity
$\bar{\sigma}$ dimensional coordinate of the wavy surface
σ dimensionless coordinate of the wavy surface, defined by Eq. (7)
τ dimensionless time parameter, defined by Eq. (7)
τ_w wall shear stress
θ dimensionless temperature, defined by Eq. (7)
ϕ dimensional nanoparticle volume fraction
Φ dimensionless nanoparticle volume fraction, defined by Eq. (7)

Subscripts

f fluid phase
p particle phase
s solid-matrix phase
w surface condition
∞ condition far away from the surface

1 Introduction

Nanofluids are multiphase colloidal suspensions which are comprised of nanometer sized metallic or non metallic particles suspended in abase liquid [1]. These liquids show a considerable increase in thermal conductivity for very small volume fraction of solid particles. Therefore, research is underway to apply nanofluids in environments where higher heat flux is encountered and the conventional fluid is not capable of achieving the desired heat transfer. Kuznetsov and Nield [2] discussed natural convection boundary-layer flow of a nanofluid past a vertical plate. The Cheng–Minkowycz problem for natural convective boundary-layer flow in a porous medium saturated by a nanofluid was studied by Nield and Kuznetsov [3]. In this article they used a model incorporates the effects of Brownian motion and thermophoresis as well as the Darcy model for the porous medium. Kuznetsov and Nield [4] developed a theory of double-diffusive nanofluid convection in porous media and applied it to investigating the onset of nanofluid convection in a horizontal layer of a porous medium saturated by a nanofluid for the case when the base fluid of the nanofluid is itself a binary fluid such as salty water. Thermal instability in a porous medium layer saturated by a nanofluid was reported by Nield and Kuznetsov [5]. They found that the critical thermal Rayleigh number can be reduced or increased by a substantial amount, depending on whether the basic nanoparticle distribution is top-heavy or bottom-heavy, by the presence of the nanoparticles. A literature survey shows that the comprehensive review of these problems was made by the authors [6–11].

In recent years, the local thermal non-equilibrium model has been given considerable attention and has been utilized in various fields [12] due to its pertinence in applications. For example, Lee and Vafai [13] employed the thermal non-equilibrium model to investigate the forced convection flow through a channel filled with a porous medium. They obtained analytical solutions for the fluid- and solid-phase temperature distributions. Mansour et al. [14] used the non-equilibrium model to study natural convection a porous cavity under the influence of thermal radiation. Chamkha et al. [15] studied the flow and heat transfer of a micropolar fluid a long a elliptic cylinder in porous media using thermal non-equilibrium model. For nanofluids, Kuznetsov and Nield [16] reported on effect of local thermal non-equilibrium on the onset of convection in a porous medium layer.

On the other hand, the study of heat transfer near irregular surfaces is of fundamental importance because it is often found in many industrial applications.

The presence of irregular surface not only alters the flow field but also alters the heat transfer characteristics. Hady et al. [17] discussed the problem of MHD free convection flow along a vertical wavy surface with heat generation or absorption effect. Kumar and Shalini [18] studied the non- Darcy free convection induced by a vertical wavy surface in a thermally stratified porous medium. Molla et al. [19] examined the natural convection flow along a vertical wavy surface with uniform surface temperature in the presence of heat generation or absorption. Hossain and Rees [20] studied the heat and mass transfer in natural convection flow along a vertical wavy surface with constant wall temperature and concentration in Newtonian fluids. Cheng [21] presented the solutions of the heat and mass transfer in natural convection flow along a vertical wavy surface in porous medium saturated with Newtonian fluids. Mahdy [22] investigated the effect of Soret and Dufour numbers on MHD non-Darcian free convection from a vertical wavy surface. Jang and Yan [23] studied the transient problem of natural convection heat and mass transfer along a wavy surface.

Motivated by the investigations mentioned above, the purpose of the present work is to consider the problem of boundary-layer free convection along a vertical wavy surface in a porous medium saturated by a nanofluid using thermal non-equilibrium model.

2 Formulation and analysis

Consider unsteady, two-dimensional flow of a nanofluid consisting of a base fluid and small nanoparticles over a vertical wavy surface. Figure 1 shows the schematic of the problem under consideration and coordinate system. In the present problem, the following assumptions have been made:

(a) The wavy surface is described by $y = \bar{\sigma}(x) = \bar{a} \cdot \sin(2\pi x/L)$.
(b) The fluid porous medium properties are assumed to be homogeneous.
(c) The effect of Brownian motion is considered.
(d) The local thermal non-equilibrium model among the particles, fluid, and solid-matrix phases is applied.
(e) The Oberbeck–Boussinesq approximation is employed.
(f) Initially, i.e. $t < 0$, the fluid, wavy surface, particle temperatures and nanoparticles volume fraction have constant values T_∞ and ϕ_∞, respectively.

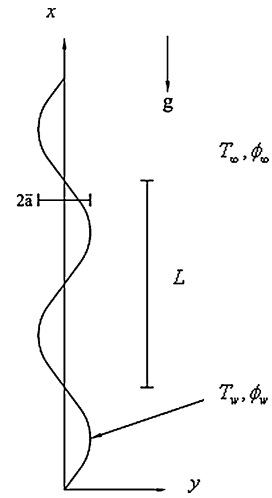

Fig. 1 Physical model and coordinates

(g) At time $t = 0$, the temperatures of fluid, wavy surface, particles and nanoparticles volume fraction changed to new values T_w and ϕ_w, respectively.

With the above assumptions, the governing equations for fluid flow are given as (see [2], [16] and [23]).

Continuity equation

$$\nabla \cdot V = 0. \tag{1}$$

Momentum equation

$$\begin{aligned}\rho_f\left[\frac{1}{\varepsilon}\frac{\partial V}{\partial t} + \frac{V\cdot\nabla V}{\varepsilon^2}\right] &= \mu\left(\nabla^2 V\right) - \nabla P - \frac{\mu}{K}V \\ &\quad + \Big[(\rho_p - \rho_{f\infty})(\phi - \phi_\infty) \\ &\quad - (1-\phi_\infty)\rho_{f\infty}\beta(T_f - T_\infty)\Big]g.\end{aligned} \tag{2}$$

Temperature equation for fluid phase

$$\begin{aligned}\varepsilon(1-\phi_\infty)(\rho C)_f\left[\frac{\partial T_f}{\partial t} + \frac{1}{\varepsilon}V\cdot\nabla T_f\right] &= \varepsilon(1-\phi_\infty)k_f\left(\nabla^2 T_f\right) \\ &\quad \times \varepsilon(1-\phi_\infty)(\rho C)_p\Big[D_B(\nabla\phi\cdot\nabla T_f) \\ &\quad + \frac{D_T}{T_\infty}(\nabla T_f\cdot\nabla T_f)\Big] \\ &\quad + h_{fp}(T_p - T_f) + h_{fs}(T_s - T_f).\end{aligned} \tag{3}$$

Temperature equation for particle phase

$$\varepsilon\phi_\infty(\rho C)_p\left[\frac{\partial T_p}{\partial t}+\frac{1}{\varepsilon}V\cdot\nabla T_p\right] = \varepsilon\phi_\infty k_p\left(\nabla^2 T_p\right)-h_{fp}(T_p-T_f). \tag{4}$$

Temperature equation for solid phase

$$(1-\varepsilon)(\rho C)_s\frac{\partial T_s}{\partial t} = (1-\varepsilon)k_s\left(\nabla^2 T_s\right)-h_{fs}(T_s-T_f). \tag{5}$$

Nanoparticle volume fraction equation

$$\frac{\partial\phi}{\partial t}+\frac{1}{\varepsilon}V\cdot\nabla\phi = D_B\left(\nabla^2\phi\right)+\left[\frac{D_T}{T_\infty}\nabla^2 T_f\right] \tag{6}$$

where, $V=(u,v)$ is the velocity vector with u and v being the x- and y-components of velocity and all the parameters appearing in the above equations are given in the nomenclatures.

Introducing the following dimensionless quantities

$$\begin{aligned}
&\bar{x}=\frac{x}{L},\qquad \bar{y}=\frac{y-\bar{\sigma}}{L}Ra^{1/4},\qquad \tau=\frac{\alpha_f t}{L^2}Ra^{1/2},\\
&\sigma=\frac{\bar{\sigma}}{L},\qquad \bar{u}=\frac{Lu}{\alpha_f}Ra^{-1/2},\\
&\bar{v}=\frac{L}{\alpha_f}Ra^{-1/4}(v-\sigma' u),\qquad \bar{p}=\frac{L^2}{\rho\alpha_f^2}Ra^{-1}p,\\
&\theta=\frac{T-T_\infty}{T_w-T_\infty},\qquad \Phi=\frac{\phi-\phi_\infty}{\phi_w-\phi_\infty}.
\end{aligned} \tag{7}$$

By using Eq. (7) and ignoring the small order terms in Ra (after allowing $Ra\to\infty$), Eqs. (1)–(6) are converted to

$$\frac{\partial\bar{u}}{\partial\bar{x}}+\frac{\partial\bar{v}}{\partial\bar{y}}=0, \tag{8}$$

$$\begin{aligned}
&\frac{1}{Pr}\left[\frac{1}{\varepsilon}\frac{\partial\bar{u}}{\partial\tau}+\frac{\bar{u}}{\varepsilon^2}\frac{\partial\bar{u}}{\partial\bar{x}}+\frac{\bar{v}}{\varepsilon^2}\frac{\partial\bar{u}}{\partial\bar{y}}\right]\\
&\quad=-\frac{1}{Pr}\left[\frac{\partial\bar{p}}{\partial\bar{x}}-\sigma' Ra^{1/4}\frac{\partial\bar{p}}{\partial\bar{y}}\right]\\
&\qquad+\left(1+\sigma'^2\right)\frac{\partial^2\bar{u}}{\partial\bar{y}^2}+\theta_f-N_r\Phi-Da^{-1}u,
\end{aligned} \tag{9}$$

$$\begin{aligned}
&\frac{1}{Pr}\frac{\sigma''}{\varepsilon^2}u^2+\sigma'(\theta_f-N_r\Phi)\\
&\quad=\frac{\sigma'}{Pr}\frac{\partial\bar{p}}{\partial\bar{x}}-\frac{(1+\sigma'^2)}{Pr}Ra^{1/4}\frac{\partial\bar{p}}{\partial\bar{y}},
\end{aligned} \tag{10}$$

$$\begin{aligned}
&\frac{\partial\theta_f}{\partial\tau}+\frac{\bar{u}}{\varepsilon}\frac{\partial\theta_f}{\partial\bar{x}}+\frac{\bar{v}}{\varepsilon}\frac{\partial\theta_f}{\partial\bar{y}}\\
&\quad=\left(1+\sigma'^2\right)\left[\frac{\partial^2\theta_f}{\partial\bar{y}^2}+N_b\frac{\partial\Phi}{\partial\bar{y}}\frac{\partial\theta_f}{\partial\bar{y}}+N_t\left(\frac{\partial\theta_f}{\partial\bar{y}}\right)^2\right]\\
&\qquad+N_{Hp}(\theta_p-\theta_f)+N_{Hs}(\theta_s-\theta_f),
\end{aligned} \tag{11}$$

$$\begin{aligned}
&\frac{\partial\theta_p}{\partial\tau}+\frac{\bar{u}}{\varepsilon}\frac{\partial\theta_p}{\partial\bar{x}}+\frac{\bar{v}}{\varepsilon}\frac{\partial\theta_p}{\partial\bar{y}}\\
&\quad=\varepsilon_p\left(1+\sigma'^2\right)\frac{\partial^2\theta_p}{\partial\bar{y}^2}-\gamma_p N_{Hp}(\theta_p-\theta_f),
\end{aligned} \tag{12}$$

$$\frac{\partial\theta_s}{\partial\tau}=\varepsilon_s\left(1+\sigma'^2\right)\frac{\partial^2\theta_s}{\partial\bar{y}^2}-\gamma_s N_{Hs}(\theta_s-\theta_f), \tag{13}$$

$$\begin{aligned}
&\frac{\partial\Phi}{\partial\tau}+\frac{\bar{u}}{\varepsilon}\frac{\partial\Phi}{\partial\bar{x}}+\frac{\bar{v}}{\varepsilon}\frac{\partial\Phi}{\partial\bar{y}}\\
&\quad=\frac{(1+\sigma'^2)}{Le}\left[\frac{\partial^2\Phi}{\partial\bar{y}^2}+\frac{N_t}{N_b}\frac{\partial^2\theta_f}{\partial\bar{y}^2}\right],
\end{aligned} \tag{14}$$

where,

$$Ra=\frac{g\beta(1-\phi_\infty)(T_w-T_\infty)L^3}{\upsilon\alpha}$$
is the Rayleigh number. (15)

$$Da=\left[\frac{k^2 g\beta(1-\phi_\infty)(T_w-T_\infty)}{\upsilon\alpha_f L}\right]^{1/2}$$
is the Darcy number. (16)

$Pr=\dfrac{\upsilon}{\alpha}$ is the Prandtl number. (17)

$Le=\dfrac{\alpha_f}{D}$ is the Lewis number. (18)

$$N_r=\frac{(\rho_p-\rho_{f\infty})(\phi_w-\phi_\infty)}{(1-\phi_\infty)\beta\rho_{f\infty}(T_w-T_\infty)}$$
is the buoyancy ratio. (19)

$$N_b=\frac{(\rho c)_p D_B(\phi_w-\phi_\infty)}{(\rho c)_f\alpha_f}$$
is the Brownian motion parameter. (20)

$$N_t=\frac{(\rho c)_p D_T(T_w-T_\infty)}{(\rho c)_f\alpha_f T_\infty}$$
is the thermophoresis parameter. (21)

$N_{Hp}=\left[\dfrac{h_{fp}^2 L\upsilon\alpha_f}{\varepsilon^2(1-\phi_\infty)^3 k_f^2(T_w-T_\infty)g\beta}\right]^{1/2}$ is Nield number for the fluid/particle interface. (22)

$N_{Hs}=\left[\dfrac{h_{fs}^2 L\upsilon\alpha_f}{\varepsilon^2(1-\phi_\infty)^3 k_f^2(T_w-T_\infty)g\beta}\right]^{1/2}$ is Nield number for the fluid/solid interface. (23)

$\gamma_p=\dfrac{(1-\phi_\infty)(\rho c)_f}{\phi_\infty(\rho c)_p}$ is the fluid/particle modified thermal capacity ratio. (24)

$\gamma_s=\dfrac{\varepsilon(1-\phi_\infty)(\rho c)_f}{(1-\varepsilon)(\rho c)_s}$ is the fluid/solid modified thermal capacity ratio. (25)

$\varepsilon_p = \dfrac{\alpha_p}{\alpha_f}$ is the fluid/particle modified thermal diffusivity ratio. (26)

$\varepsilon_s = \dfrac{\alpha_s}{\alpha_f}$ is the fluid/solid modified thermal diffusivity ratio. (27)

In the current problem, the pressure gradient $\frac{\partial \bar{p}}{\partial \bar{x}}$ is zero [23]. Therefore, Eqs. (9) and (10) can be reduced to the following equation:

$$\frac{1}{Pr}\left[\frac{1}{\varepsilon}\frac{\partial \bar{u}}{\partial \tau} + \frac{\bar{u}}{\varepsilon^2}\frac{\partial \bar{u}}{\partial \bar{x}} + \frac{\bar{v}}{\varepsilon^2}\frac{\partial \bar{u}}{\partial \bar{y}}\right] = \left(1+\sigma'^2\right)\frac{\partial^2 \bar{u}}{\partial \bar{y}^2} - Da^{-1}u + \frac{1}{1+\sigma'^2}\left(\theta_f - N_r\Phi - \frac{\bar{u}^2\sigma'\sigma''}{Pr\varepsilon^2}\right). \tag{28}$$

It is noticeable that σ' and σ'' indicate the first and second differentiations of σ with respect to $\bar{x}$. In addition, the singularity at the leading edge can be removed by introducing the following transformation.

$$X = \bar{x}, \qquad Y = \frac{\bar{y}}{(4\bar{x})^{1/4}}, \qquad U = \frac{\bar{u}}{(4\bar{x})^{1/2}}, \qquad V = (4\bar{x})^{1/4}\bar{v}. \tag{29}$$

Equations (8), (11), (12), (13), (14) and (28) become:

$$4X\frac{\partial U}{\partial X} + 2U - Y\frac{\partial U}{\partial Y} + \frac{\partial V}{\partial Y} = 0, \tag{30}$$

$$\frac{1}{Pr}\left[\frac{1}{\varepsilon}\frac{\partial U}{\partial \tau} + \frac{1}{\varepsilon^2}\left(4XU\frac{\partial U}{\partial X} + (V-UY)\frac{\partial U}{\partial Y} + \left(2 + \frac{4X\sigma'\sigma''}{1+\sigma'^2}\right)U^2\right)\right] = \left(1+\sigma'^2\right)\frac{\partial^2 U}{\partial Y^2} - \frac{2\sqrt{X}}{Da}U + \frac{1}{1+\sigma'^2}(\theta_f - N_r\Phi), \tag{31}$$

$$\frac{\partial \theta_f}{\partial \tau} + \frac{1}{\varepsilon}\left(4XU\frac{\partial \theta_f}{\partial X} + (V-UY)\frac{\partial \theta_f}{\partial Y}\right) = \left(1+\sigma'^2\right)\left[\frac{\partial^2 \theta_f}{\partial Y^2} + N_b\frac{\partial \Phi}{\partial Y}\frac{\partial \theta_f}{\partial Y} + N_t\left(\frac{\partial \theta_f}{\partial Y}\right)^2\right] + N_{Hp}(\theta_p - \theta_f) + N_{Hs}(\theta_s - \theta_f), \tag{32}$$

$$\frac{\partial \theta_p}{\partial \tau} + \frac{1}{\varepsilon}\left(4XU\frac{\partial \theta_p}{\partial X} + (V-UY)\frac{\partial \theta_p}{\partial Y}\right) = \varepsilon_p\left(1+\sigma'^2\right)\frac{\partial^2 \theta_p}{\partial Y^2} - \gamma_p N_{Hp}(\theta_p - \theta_f), \tag{33}$$

$$\frac{\partial \theta_s}{\partial \tau} = \varepsilon_s\left(1+\sigma'^2\right)\frac{\partial^2 \theta_s}{\partial \bar{y}^2} - \gamma_s N_{Hs}(\theta_s - \theta_f), \tag{34}$$

$$\frac{\partial \Phi}{\partial \tau} + \frac{1}{\varepsilon}\left(4XU\frac{\partial \Phi}{\partial X} + (V-UY)\frac{\partial \Phi}{\partial Y}\right) = \frac{(1+\sigma'^2)}{Le}\left[\frac{\partial^2 \Phi}{\partial Y^2} + \frac{N_r}{N_t}\frac{\partial^2 \theta_f}{\partial Y^2}\right]. \tag{35}$$

The dimensionless forms of the boundary are

$$\begin{aligned} &Y = 0: \quad U = V = 0, \quad \theta_f = \theta_p = \theta_s = 1, \quad \Phi = 1, \\ &Y \to \infty: \quad U \to 0, \quad \theta_f \to 0, \quad \theta_p \to 0, \\ &\theta_s \to 0, \quad \Phi \to 0. \end{aligned} \tag{36}$$

The local Nusselt number for fluid, particle and solid phases are defined, respectively, as:

$$Nu_{xf} = \frac{h_f x}{k_f} = -\left[\frac{X^3 Ra}{4}\right]^{1/4}\left(1+\sigma'^2\right)^{1/2}\left.\frac{\partial \theta_f}{\partial Y}\right|_{Y=0}, \tag{37}$$

$$Nu_{xp} = \frac{h_p x}{k_p} = -\left[\frac{X^3 Ra}{4}\right]^{1/4}\left(1+\sigma'^2\right)^{1/2}\left.\frac{\partial \theta_p}{\partial Y}\right|_{Y=0}, \tag{38}$$

$$Nu_{xs} = \frac{h_s x}{k_s} = -\left[\frac{X^3 Ra}{4}\right]^{1/4}\left(1+\sigma'^2\right)^{1/2}\left.\frac{\partial \theta_s}{\partial Y}\right|_{Y=0}. \tag{39}$$

The local Sherwood number is defined by:

$$Sh_x = \frac{h_D x}{D} = -\left[\frac{X^3 Ra}{4}\right]^{1/4}\left(1+\sigma'^2\right)^{1/2}\left.\frac{\partial \Phi}{\partial Y}\right|_{Y=0}. \tag{40}$$

The local skin friction coefficient C_{fx} is defined as:

$$C_{fx} = \frac{2\tau_w}{\rho \tilde{U}^2} \tag{41}$$

where $\tilde{U} = \frac{L}{\alpha_f Ra^{1/2}}$ is characteristic velocity and the shearing stress on the wavy surface is

$$\tau_w = \left[\mu\left(\frac{\partial v}{\partial x} + \frac{\partial u}{\partial y}\right)\right]_{y=0}. \tag{42}$$

Substituting Eq. (42) into Eq. (41) yields:

$$C_{fx} = 2Pr\left(\frac{4X}{Ra}\right)^{1/4}\left(1+\sigma'^2\right)\left[\frac{\partial U}{\partial Y}\right]_{Y=0}. \tag{43}$$

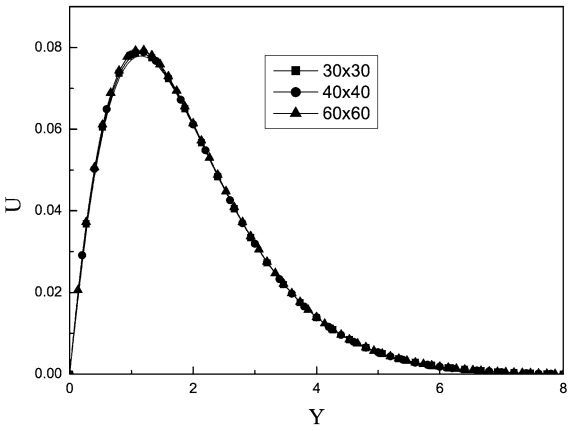

Fig. 2 Grid independence results at ($A = 0.1$, $Da = 1$, $Le = 10$, $Pr = 10$, $N_b = 0.5$, $N_r = 0.5$, $N_t = 0.5$, $N_{Hp} = 1$, $N_{Hs} = 10$)

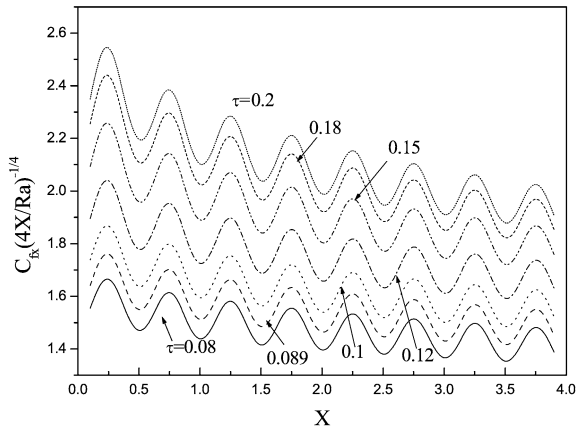

Fig. 3 Effects of dimensionless time parameter τ on the local skin friction coefficient at ($A = 0.1$, $Da = 1$, $Pr = 10$, $Le = 10$, $N_b = 0.5$, $N_r = 0.5$, $N_t = 0.5$, $N_{Hp} = 1$, $N_{Hs} = 1$)

3 Results and discussion

In order to solve these unsteady, non-linear coupled Eqs. (32) to (35) under the conditions (36), an implicit finite difference scheme of Crank-Nicolson type has been employed. This method has been extensively developed in recent years and remains one of the most reliable procedures for solving partial differential equation systems. The details of this method can be found in recent article reported by Chamkha et al. [24]. The steady-state criteria for the relative deviations of the variables U, V, θ_f, θ_p, θ_s and Φ between two time intervals is less than 10^{-5}. Figure 2 shows an accuracy tests using the finite difference method using three sets of grids: 30×30, 40×40, 60×60. A 40×40 uniform grid is found to meet the requirements of both the grid independence study and the computational time limits. The numerical method was implemented in a FORTRAN software. The obtained results are plotted in 2D and 3D graphs by using ORIGIN6 software and MATLAB software, respectively. The results of the present problem are presented in Figs. 3–16. In all the results to be reported below, the values of N_t, N_b, N_r, Pr and Le are taken to be 0.5, 0.5, 0.5, 10 and 10 respectively, as Kuznetsov and Nield [2]. Also, values of ε, ε_p, ε_s, γ_p, γ_s and Da are fixed at 0.4, 1, 1, 1, 1 and 1, respectively (Mansour et al. [14] and Chamkha et al. [15]).

Figures 3–7 show the effects of dimensionless time parameter τ on the local skin friction coefficient, local Sherwood number, local Nusselt for fluid phase, local Nusselt number for particle phase and local Nusselt number for solid phase, respectively. It is found

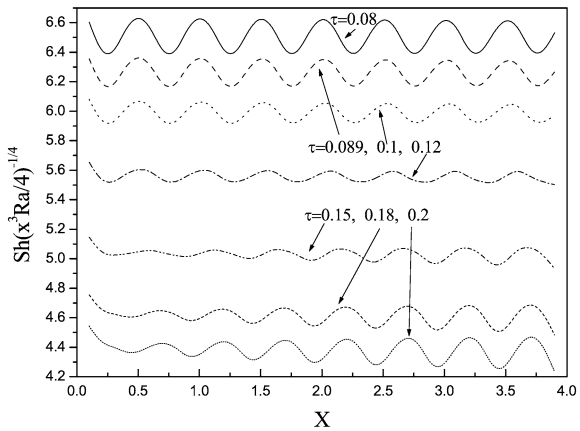

Fig. 4 Effects of dimensionless time parameter τ on the local Sherwood number at ($A = 0.1$, $Da = 1$, $Pr = 10$, $Le = 10$, $N_b = 0.5$, $N_r = 0.5$, $N_t = 0.5$, $N_{Hp} = 1$, $N_{Hs} = 1$)

that, at the initial transients, the hydrodynamic boundary layer thickness and the wall shear stress take small values. The reason for that is the buoyancy-induced flow velocity is relatively low at the initial transients. As the time parameter τ increases the hydrodynamic boundary layer thickness and the wall shear stress increase, which in turn, the skin-friction coefficient increases as well. Also, the maximum values of skin-friction coefficient arises beside the wall but these values decreases as X increases (far way from the wall). Regarding the local Sherwood number, local Nusselt for fluid phase, local Nusselt number for particle phase and local Nusselt number for solid phase, it decrease with increase the dimensionless time parameter. In ad-

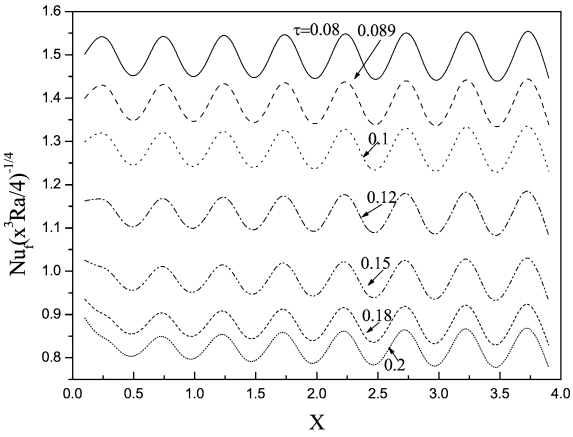

Fig. 5 Effects of dimensionless time parameter τ on the local Nusselt for fluid phase at ($A = 0.1$, $Da = 1$, $Pr = 10$, $Le = 10$, $N_b = 0.5$, $N_r = 0.5$, $N_t = 0.5$, $N_{Hp} = 1$, $N_{Hs} = 1$)

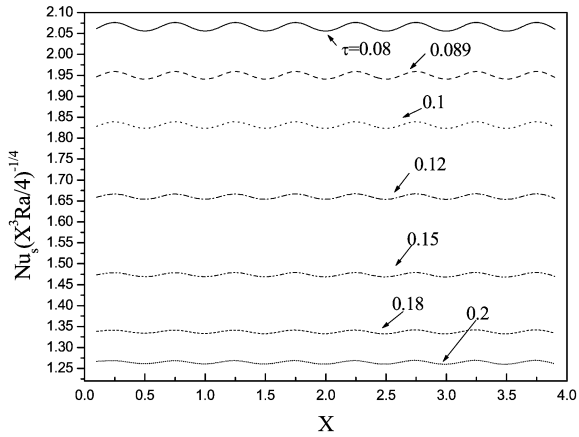

Fig. 7 Effects of dimensionless time parameter τ on the local Nusselt number for solid phase at ($A = 0.1$, $Da = 1$, $Pr = 10$, $Le = 10$, $N_b = 0.5$, $N_r = 0.5$, $N_t = 0.5$, $N_{Hp} = 1$, $N_{Hs} = 1$)

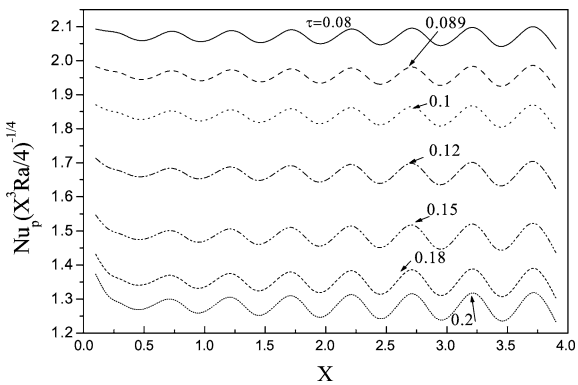

Fig. 6 Effects of dimensionless time parameter τ on the local Nusselt number for particle phase at ($A = 0.1$, $Da = 1$, $Pr = 10$, $Le = 10$, $N_b = 0.5$, $N_r = 0.5$, $N_t = 0.5$, $N_{Hp} = 1$, $N_{Hs} = 1$)

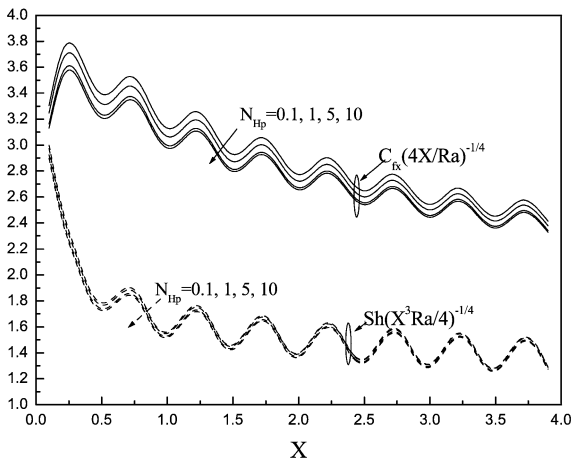

Fig. 8 Effects of Nield number for the fluid/particle interface N_{Hp} on the steady profiles of local skin-friction coefficient and local Sherwood number at ($A = 0.1$, $Da = 1$, $Pr = 10$, $Le = 10$, $N_b = 0.5$, $N_r = 0.5$, $N_t = 0.5$, $N_{Hs} = 1$)

dition, at the initial transients the maximum values of the local Sherwood number, local Nusselt for fluid phase, local Nusselt number for particle phase and local Nusselt number for solid phase remain the same. But, as the time proceeds, these values decrease as X increases. All these behaviors are plotted in Figs. 3–7 with referenced case $A = 0.1$, $Da = 1$, $Pr = 10$, $Le = 10$, $N_b = 0.5$, $N_r = 0.5$, $N_t = 0.5$, $N_{Hp} = 1$, $N_{Hs} = 1$.

The effects of thermal nonequilibrium between the fluid and particle represented by the variations of Nield number for the fluid/particle interface N_{Hp} on the steady profiles of local skin-friction coefficient and local Sherwood number are plotted in Fig. 8. The results show that, increasing in the Nield number for the fluid/particle interface N_{Hp} leads to a decreasing the intensity of buoyancy and hence the flow intensity, which in turn, the skin-friction coefficient decreases as well. The same behavior is observed for the local Sherwood number. In addition, the variations of N_{Hp} have a significant effects on the local Nusselt number for fluid, particle and sold-matrix phases. This clearly can be found in Fig. 9. The Nusselt number for fluid and solid-matrix phases increase as N_{Hp} increases whereas, the Nusselt number for particle phase takes the inverse behaviors.

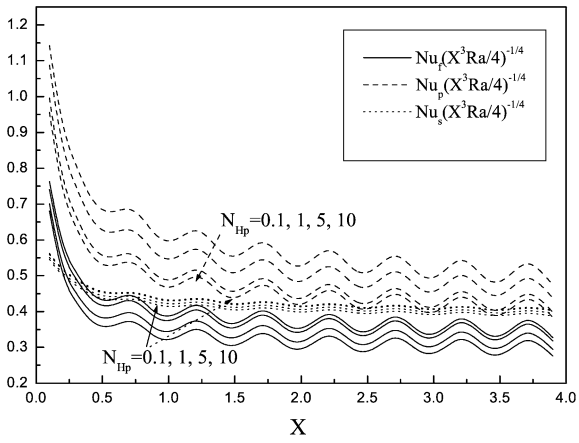

Fig. 9 Effects of Nield number for the fluid/particle interface N_{Hp} on the steady profiles of local Nusselt numbers for fluid, particle and solid phases at ($A = 0.1$, $Da = 1$, $Pr = 10$, $Le = 10$, $N_b = 0.5$, $N_r = 0.5$, $N_t = 0.5$, $N_{Hs} = 1$)

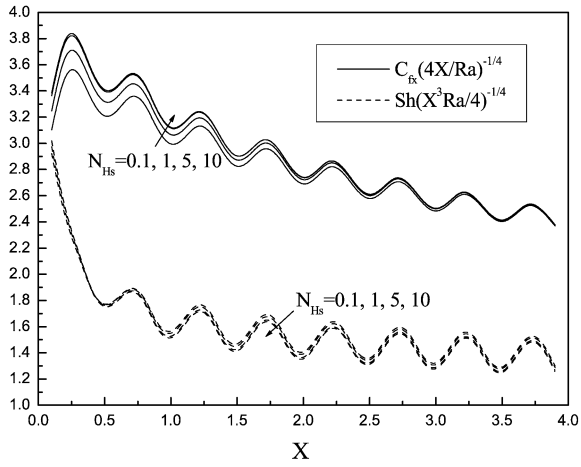

Fig. 10 Effects of Nield number for the fluid/solid interface N_{Hs} on the steady profiles of local skin-friction coefficient and local Sherwood number at ($A = 0.1$, $Da = 1$, $Pr = 10$, $Le = 10$, $N_b = 0.5$, $N_r = 0.5$, $N_t = 0.5$, $N_{Hp} = 1$)

With the help of Figs. 10 and 11, the effects of thermal nonequilibrium between the fluid and solid phases at the steady state can be observed. The variations of Nield number for the fluid/solid interface N_{Hs} represent this influence. The referenced case for these figures is $A = 0.1$, $Da = 1$, $Pr = 10$, $Le = 10$, $N_b = 0.5$, $N_r = 0.5$, $N_t = 0.5$, $N_{Hp} = 1$. The results show that, increasing in N_{Hs} results in an increase in the thermal nonequilibrium state between the fluid and solid phases. This can be found clearly in the profiles of skin-friction coefficient and local Nusselt number for

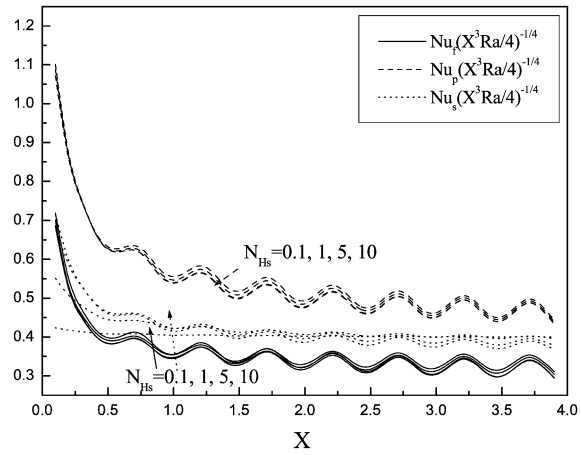

Fig. 11 Effects of Nield number for the fluid/solid interface N_{Hs} on the steady profiles of local Nusselt numbers for fluid, particle and solid phases at ($A = 0.1$, $Da = 1$, $Pr = 10$, $Le = 10$, $N_b = 0.5$, $N_r = 0.5$, $N_t = 0.5$, $N_{Hp} = 1$)

solid matrix. These profiles have significant influences with variations of N_{Hs} beside the wall but far away from the wall these influences is little observed. This can be attributed to the difference between the fluid temperature and solid-matrix temperature which decrease as X increases (far away from the wall). In addition, increasing in N_{Hs} leads to increase both of skin-friction, local Nusselt number for fluid phase and local Nusselt number for solid phase, however, it decrease local Sherwood number and local Nusselt number for particle phase.

Figures 12–16 display the axial velocity component U, nanoparticle volume fraction Φ, fluid temperature θ_f, particle temperature θ_p and solid-matrix temperature θ_s as a function of the axial and transverse coordinates at the steady-state case. It is clear that, the effect of sinusoidal variation of the wavy surface is significant through the profiles of the velocity, nanoparticle volume fraction, fluid temperature, particle temperature and solid matrix temperature. Also, the amplitude of the velocity component takes its maximum beside the wall and it decreases as X increases. However, the amplitudes of nanoparticle volume fraction, fluid temperature, particle temperature and solid matrix temperature remain the same. These profiles can be found in Figs. 12–16 with referenced case $A = 0.1$, $Da = 1$, $Pr = 10$, $Le = 10$, $N_b = 0.5$, $N_r = 0.5$, $N_t = 0.5$, $N_{Hp} = 1$, $N_{Hs} = 1$.

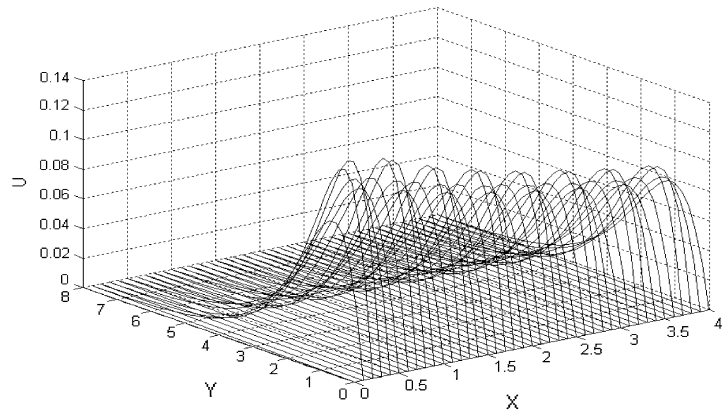

Fig. 12 Axial velocity profiles at ($A = 0.1$, $Da = 1$, $Pr = 10$, $Le = 10$, $N_b = 0.5$, $N_r = 0.5$, $N_t = 0.5$, $N_{Hp} = 1$, $N_{Hs} = 1$)

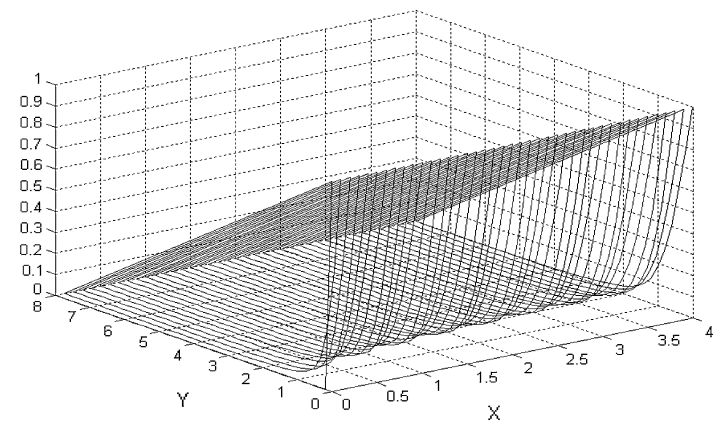

Fig. 13 Profiles of nanoparticle volume fraction Φ at ($A = 0.1$, $Da = 1$, $Pr = 10$, $Le = 10$, $N_b = 0.5$, $N_r = 0.5$, $N_t = 0.5$, $N_{Hp} = 1$, $N_{Hs} = 1$)

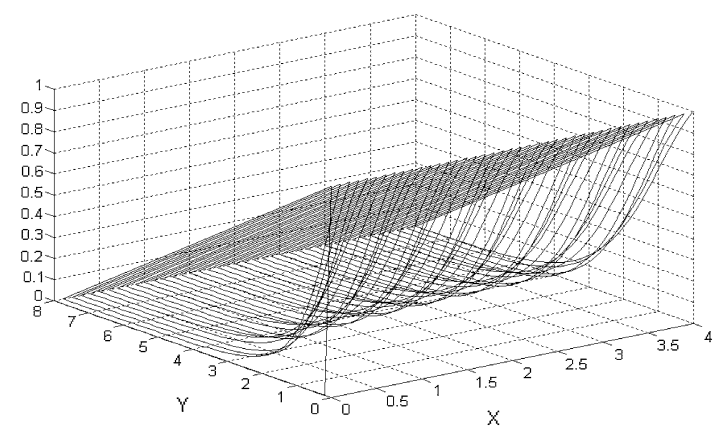

Fig. 14 Fluid temperature profiles θ_f at ($A = 0.1$, $Da = 1$, $Pr = 10$, $Le = 10$, $N_b = 0.5$, $N_r = 0.5$, $N_t = 0.5$, $N_{Hp} = 1$, $N_{Hs} = 1$)

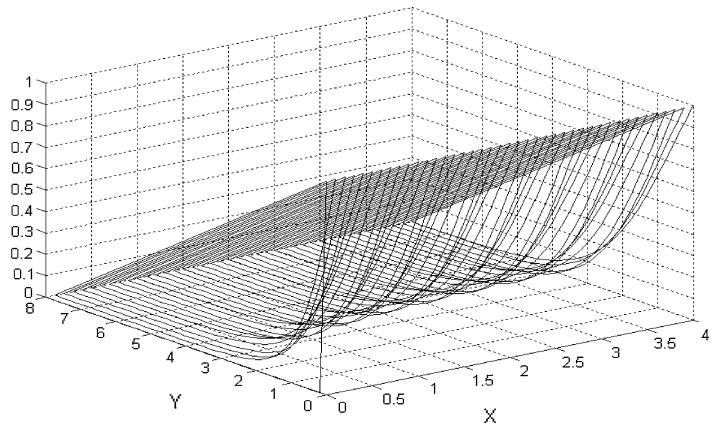

Fig. 15 Particle temperature profiles θ_p at ($A = 0.1$, $Da = 1$, $Pr = 10$, $Le = 10$, $N_b = 0.5$, $N_r = 0.5$, $N_t = 0.5$, $N_{Hp} = 1$, $N_{Hs} = 1$)

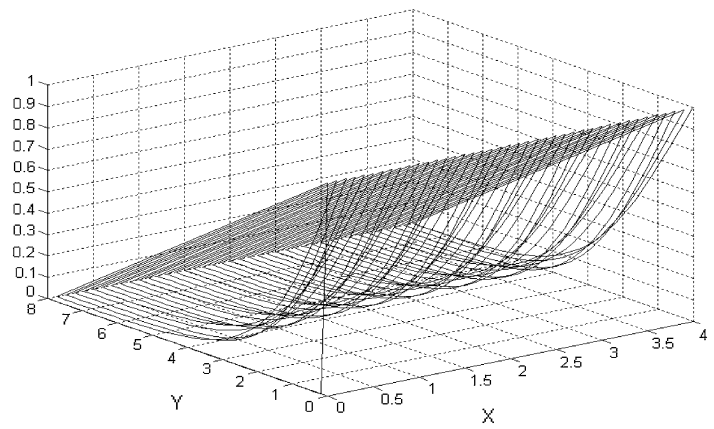

Fig. 16 Solid-matrix temperature profiles θ_s at ($A = 0.1$, $Da = 1$, $Pr = 10$, $Le = 10$, $N_b = 0.5$, $N_r = 0.5$, $N_t = 0.5$, $N_{Hp} = 1$, $N_{Hs} = 1$)

4 Conclusions

In the present paper, heat transfer by natural convection of a nanofluid over a wavy surface using thermal nonequilibrium model was studied. The nonequilibrium state was taken among fluid, particle and solid phases. A numerical solution of the problem was obtained using finite-difference method with Crank-Nicolson type. A parametric study was performed to examine the effects of dimensionless time parameter, Nield number for the fluid/particle interface and Nield number for the fluid/solid interface on the flow and heat transfer characteristics. From this investigation, we can draw the following conclusions:

- The local skin-friction coefficient increases monotonically as the dimensionless time parameter increases, whereas, the local Sherwood number, local Nusselt numbers for fluid, particle and solid phases decreases as the dimensionless time parameter increases.
- Increasing in the Nield number for the fluid/particle interface leads to increase the difference between the fluid and particle temperatures which increase the nonequilibrium state between the fluid and particle.
- Both of Nusselt numbers for fluid and solid phases increase as Nield number for the fluid/particle interface increases whereas, the skin-friction coefficient, Sherwood number and Nusselt number for particle phase take the inverse behaviors.
- Increasing in the Nield number for the fluid/solid interface leads to increase skin-friction coefficient, Nusselt number for fluid phase and Nusselt number

for solid phase, whereas, the Sherwood number and Nusselt number for particle phase take the opposite behaviors.

References

1. Choi S (1995) Enhancing thermal conductivity of fluids with nanoparticles, vol 66. ASME, New York, pp 99–105
2. Kuznetsov AV, Nield DA (2010) Natural convection boundary layer flow of a nanofluid past a vertical plate. Int J Therm Sci 49:243–247
3. Nield DA, Kuznetsov AV (2009) The Cheng–Minkowycz problem for natural convective boundary-layer flow in a porous medium saturated by a nanofluid. Int J Heat Mass Transf 52:5792–5795
4. Kuznetsov AV, Nield DA (2010) The onset of double-diffusive nanofluid convection in a layer of a saturated porous medium. Transp Porous Media 85:941–951
5. Nield DA, Kuznetsov AV (2009) Thermal instability in a porous medium layer saturated by a nanofluid. Int J Heat Mass Transf 52:5796–5801
6. Chamkha AJ, Gorla RSR, Ghodeswar K Non-similar solution for natural convective boundary layer flow over a sphere embedded in a porous medium saturated with a nanofluid. Transp Porous Media. doi:10.1007/s11242-010-9601-0
7. Tzou DY (2008) Instability of nanofluids in natural convection. ASME J Heat Transf 130:072401
8. Tzou DY (2008) Thermal instability of nanofluids in natural convection. Int J Heat Mass Transf 51:2967–2979
9. Kim J, Kang YT, Choi CK (2004) Analysis of convective instability and heat transfer characteristics of nanofluids. Phys Fluids 16:2395–2401
10. Kim J, Choi CK, Kang YT, Kim MG (2006) Effects of thermodiffusion and nanoparticles on convective instabilities in binary nanofluids. Nanoscale Microscale Thermophys Eng 10:29–39
11. Kim J, Kang YT, Choi CK (2007) Analysis of convective instability and heat transfer characteristics of nanofluids. Int J Refrig 30:323–328
12. Quintard M (1998) Modelling local non-equilibrium heat transfer in porous media. In: Proceedings of the 11th international heat transfer conference, vol 1, pp 1279–285
13. Lee DY, Vafai K (1999) Analytical characterization and conceptual assessment of solid and fluid temperature differentials in porous media. Int J Heat Mass Transf 42:423–435
14. Mansour MA, Abd El-Aziz MM, Mohamed RA, Ahmed SE (2011) Numerical simulation of natural convection in wavy porous cavities under the influence of thermal radiation using a thermal non-equilibrium model. Transp Porous Media 86:585–600
15. Chamkha AJ, Mohamed RA, Ahmed SE (2009) Free convective flow of a micropolar fluid along an elliptic cylinder in porous media using the thermal non-equilibrium model. Int J Ind Math 1:294–305
16. Kuznetsov AV, Nield DA (2010) Effect of local thermal non-equilibrium on the onset of convection in a porous medium layer saturated by a nanofluid. Transp Porous Media 83:425–436
17. Hady FM, Mohamed RA, Mahdy A (2006) MHD free convection flow along a vertical wavy surface with heat generation or absorption effect. Int Commun Heat Mass Transf 33:1253–1263
18. Rathish Kumar BV, Shalini (2004) Non-Darcy free convection induced by a vertical wavy surface in a thermally stratified porous medium. Int J Heat Mass Transf 47:2353–2363
19. Molla MM, Hossain MA, Lun SY (2004) Natural convection flow along a vertical wavy surface with uniform surface temperature in presence of heat generation/absorption. Int J Therm Sci 43:157–163
20. Hossain MA, Rees DAS (1999) Combined heat and mass transfer in natural convection flow from a vertical wavy surface. Acta Mech 136:133–141
21. Cheng CY (2000) Natural convection heat and mass transfer near a vertical wavy surface with constant wall temperature and concentration in a porous medium. Int Commun Heat Mass Transf 27:1143–1154
22. Mahdy A (2009) MHD non-Darcian free convection from a vertical wavy surface embedded in porous media in the presence of Soret and Dufour effect. Int Commun Heat Mass Transf 36:1067–1074
23. Jang J-H, Yan W-M (2004) Transient analysis of heat and mass transfer by natural convection over a vertical wavy surface. Int J Heat Mass Transf 47:3695–3705
24. Chamkha AJ, Mohamed RA, Ahmed SE (2011) Unsteady MHD natural convection from a heated vertical porous plate in a micropolar fluid with Joule heating, chemical reaction and radiation effects. Meccanica 46:399–411